RSC Advances

PAPER

View Article Online
View Journal | View Issue

Check for updates

Cite this: *RSC Adv.*, 2020, **10**, 2566

Positive and negative birefringence in packed films of binary spherical colloidal particles†

Kai Inoue [a] and Susumu Inasawa *[ab]

Received 20th November 2019
Accepted 6th January 2020

DOI: 10.1039/c9ra09704j

rsc.li/rsc-advances

We have investigated the birefringence in packed films of binary spherical colloidal particles. Particulate films were obtained by drying a mixed suspension of colloidal particles with two different diameters. We observed positive and negative birefringence depending on the diameters and volume ratios of the large and small particles. When the diameters of the large and small particles were similar, the films showed positive birefringence. However, negative birefringence or weakening of positive birefringence was observed in films with a large diameter ratio and an optimal volume fraction of large particles. The large particles were embedded in packed small particles in the negative and weakened positive birefringent films. We propose a packing structure in which a single shell layer of small particles formed around a large particle. Using this model, we estimated the required volume ratio of large particles, and it was in good agreement with the optimal volume fraction. The relation between the packing structure of the binary colloidal particles and the birefringence is discussed.

Open Access Article. Published on 14 January 2020. Downloaded on 9/23/2024 2:41:28 AM.
This article is licensed under a Creative Commons Attribution-NonCommercial 3.0 Unported Licence.

1. Introduction

Deposition of particulate films by drying colloidal suspensions has been widely investigated because of its variety of applications and manufacturing techniques in industry, such as for paints,[1] optical films,[2–4] electrodes,[5,6] inkjet printing,[7] and the dip-coating process.[8] Mixing different sized particles is frequently used to prepare slurries. Therefore, drying colloidal suspensions with a binary size distribution has attracted much attention for a decade.[9] One of the most attractive issues is the segregation or stratification phenomenon of small or large particles that occurs during drying.[10–13] Sun *et al.*[14] investigated drying of a sessile droplet of a binary suspension. They found that segregation was enhanced as the wettability of the substrate increased, which was explained by the interplay of the evaporative flow and particle–substrate interaction near the contact line. Patil *et al.*[15] reported that self-sorting of binary colloidal particles was observed around the contact line of a drying sessile droplet. The patterns in the deposited particles significantly depended on the substrate temperature and particle-diameter ratio. Formation of three types of depositions was demonstrated: an inner deposition of mixed particles and ring-like depositions with and without self-sorting. Furthermore, not only stratification, but also fingering patterns induced by inward Marangoni flow that was more dominant than the outward coffee ring effect have been observed.[16] Other research groups have also extensively investigated segregation of binary colloidal particles during drying, both experimentally and numerically.[17–19] These fundamental studies contribute to development of a novel method with which a patterned deposition of binary colloidal particles can be obtained by simple drying of binary colloidal suspensions.

The optical properties of particulate films of binary colloidal particles are interesting because of their tunable color and nonfading properties.[20,21] For example, Foster *et al.*[22] reported structural coloration using binary colloidal suspensions and carbon black. Films produced by drop casting of suspensions showed different structural colors (white, blue, or green) by changing the weight ratio of carbon black. Such structural colors were produced by suppression of wavelength-independent scattering. Kawamura *et al.*[23,24] reported tuning of the structural color by changing the mixing ratio of two core–shell particles. In addition, a monolayer of binary crystals of polystyrene particles prepared by ethanol-assisted self-assembly also showed opal-like structural colors.[25] These reports reveal that the appearance of particulate films is affected by the diameters and mixing ratio of the binary particles.

While much attention has been paid to exhibition of the structural color using binary colloidal particles, we believe that the optical anisotropy of packed films is also important. It is well known that birefringence emerges in films of anisotropic materials, such as nanorods and nanotubes.[26,27] Directionally aligned rods or nanotubes cause optical anisotropy. The refractive index parallel to the alignment differs from that in other directions, such as vertical to the alignment. For such

[a]*Graduate School of Bio-Applications and Systems Engineering, Tokyo University of Agriculture and Technology, 2-24-16 Nakacho, Koganei, Tokyo 184-8588, Japan. E-mail: inasawa@cc.tuat.ac.jp; Fax: +81-42-388-7798; Tel: +81-42-388-7105*

[b]*Department of Chemical Engineering, Tokyo University of Agriculture and Technology, 2-24-16 Nakacho, Koganei, Tokyo 184-8588, Japan*

† Electronic supplementary information (ESI) available. See DOI: 10.1039/c9ra09704j

This journal is © The Royal Society of Chemistry 2020

Open Access Article. Published on 14 January 2020. Downloaded on 9/23/2024 2:41:28 AM.
This article is licensed under a Creative Commons Attribution-NonCommercial 3.0 Unported Licence.

aligned anisotropic particles, a theoretical model can be applied to explain birefringence.[28] This optical anisotropy is not caused by only the morphology of the material. Even particulate films of "spherical" particles show birefringence.[1,29–31] Nanometer-scale anisotropy in the packing structure, in which packed particles are directionally compressed by drying-induced packing, has been proposed to explain this phenomenon. In birefringence, a well-ordered packing structure of particles is not necessary,[30] which differs from the structural color. Birefringence of a binary-particulate film has been briefly reported in a previous study.[30] However, there is still a lack of fundamental understanding about how the sizes and mixing ratio of the binary particles affect the optical anisotropy of the films. In this study, we systematically investigated the sizes and mixing ratio of binary colloidal particles. We revealed that positive and negative birefringence occurs depending on the ratio. The effects of the particle sizes and mixing ratio on the birefringence are discussed.

2. Experimental

2.1 Preparation of binary suspensions

We used commercial colloidal silica suspensions in water. Five colloidal suspensions, Snowtex-XS, Snowtex-30, Snowtex-30L, MP-1040, and MP-2040, were purchased from Nissan Chemical Industries Inc. (Tokyo, Japan). We also used another colloidal silica suspension, Ludox TM-40, Sigma-Aldrich Co., LLC (St. Louis, US). The fundamental information about the suspensions, including the weight fraction of particles to suspensions, diameter, and solution pH, is summarized in Table 1. The data was provided by the suppliers. We also measured the zeta potentials of the suspended particles by dynamic light scattering (DLS, Zetasizer Nano-ZS, Malvern Panalytical Ltd., Malvern, UK). All of the colloidal particles were negatively charged and we consider that they were initially well dispersed. Binary suspensions were prepared by mixing two of the suspensions. The diameters and mixing volume ratios of the binary suspensions are summarized in Table 2. After we mixed two suspensions by hand, they were further mixed in an ultrasonic bath for several minutes. We define the ratio of the larger diameter particles (d_L) to the smaller diameter particles (d_S) as $\alpha = d_L/d_S$. As shown in Table 2, we changed α and the volume fraction of large particles (φ_L) in sample preparation. We defined φ_L as the volume fraction of large particles to the total volume of dried binary particles. In all of the binary suspensions, the initial weight fraction of mixed solid particles was set to 20 wt% to the total weight of suspensions so that we were able to observe a whole dried particulate film clearly. We confirmed that the initial weight fraction of binary particles did not affect signs of the birefringence.

2.2 Film formation and observation of the particulate films

A 2 μl aliquot of the suspension was cast onto a glass plate (NEO microscope cover glass, Matsunami Glass, Osaka, Japan). The suspensions were mainly dried at room temperature (approx. 25 °C). The particulate films obtained by droplet drying were observed by optical microscopy (Eclipse Ti2-E and AZ100, Nikon, Tokyo, Japan). We observed the films in transmission mode. For birefringent observation, the particulate film was inserted between two polarization plates (SPF-50C-32, Sigma Koki, Tokyo, Japan), which were set for crossed polarization. We also inserted a compensator (HI-RETAX-1λ, Luceo, Tokyo, Japan) to visualize the birefringent color. The slow axis of the compensator was oriented 45° to the polarization directions. Birefringent observation of the packed films of mono-modal colloidal particles is summarized in Fig. S1 in the ESI.† The surfaces of the particulate films were observed by field-emission scanning electron microscopy (FE-SEM, JSM-6330FS, JEOL, Tokyo, Japan). Thickness of formed films was measured by a confocal laser displacement meter (LT9500, Keyence Co., Tokyo, Japan). As seen in Fig. 1, there was a variation in film thickness of formed samples but the maximum film thickness in each sample was typically 110 ± 10 μm. We note that variation in film thickness did not affect signs of birefringence in particulate films.

3. Results and discussion

3.1 Positive and negative birefringence

Photographs of a particulate film made of binary particles (α = 2.2) with $\varphi_L = 0.7$ are shown in Fig. 1a–c. The pale yellow packed film in the transmission image in Fig. 1a shows the maltase pattern under crossed-nicols observation (Fig. 1b). This pattern means that the packed film had the birefringent property. The difference in the refractive indices of the packed film was visualized by insertion of a compensator in crossed-nicols observation (Fig. 1c). The color pattern in which the first and third quadrants are blue and the second and forth quadrants are orange-red means that the refractive index of the packed

Table 1 Characteristics of the colloidal silica suspensions used in the experiments

Sample	Weight fraction of suspended particles [%]	Diameter (d) [nm]	Zeta potential [mV]	pH
Snowtex-XS	20.4	5	−39	9.2
Snowtex-30	30.3	12	−30	10.0
Ludox-TM40	40.0	20	−37	9.0
Snowtex-30L	29.4	45	−38	11.0
MP-1040	40.0	100	−45	9.4
MP-2040	40.5	200	−40	9.5

Open Access Article. Published on 14 January 2020. Downloaded on 9/23/2024 2:41:28 AM.
This article is licensed under a Creative Commons Attribution-NonCommercial 3.0 Unported Licence.

Table 2 Binary colloidal suspensions prepared in the experiments. We prepared all binary suspensions so that the weight fraction of initially suspended binary particles in suspensions was 20 wt%. In this table, φ_L was defined as the volume fraction of large particles to the total volume of dried binary particles

No.	α [—]	d_L [nm]	d_S [nm]	Initial weight fraction of mixed particles [%]	Volume fraction of large particles (φ_L) [—]
1	40.0	200	5	20	0.1, 0.3, 0.5, 0.7, 0.9
2	16.7	200	12		
3	10.0	200	20		
4	4.4	200	45		
5	2.0	200	100		
6	20.0	100	5		
7	8.3	100	12		
8	5.0	100	20		
9	2.2	100	45		

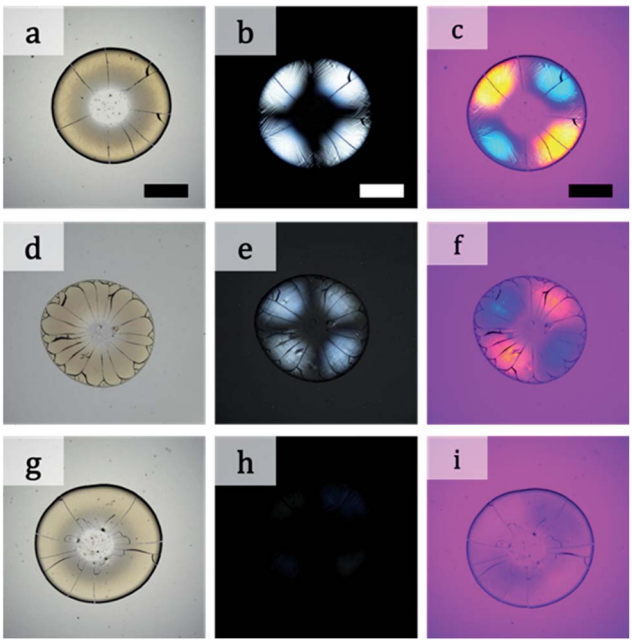

Fig. 1 Optical micrographs of films of binary colloidal particles observed (a), (d), and (g) in transmission mode, (b), (e), and (h) under crossed polarizers, and (c), (f), and (i) under crossed polarizers with a compensator for (a)–(c) $\alpha = 2.0$, (d)–(f) $\alpha = 8.3$, and (g)–(i) $\alpha = 5.0$. All of the scale bars are 500 μm.

film in the radial direction is larger than that in the circumferential direction. This is a typical feature of positive spherulites. The mixture of particles with diameters of 100 and 12 nm ($\alpha = 8.3$) showed a different pattern. Although the packed film of mixture particles appeared similar in both transmission and crossed-nicols observation (Fig. 1d and e), the color pattern was different. The first and third quadrants were orange-red and the other two quadrants appeared blue (Fig. 1f). This is a feature of negative spherulites, in which the refractive index in the circumferential direction is larger than that in the radial direction. Another packed film composed of 100 and 20 nm particles ($\alpha = 5.0$, Fig. 1g) showed no maltase pattern in the crossed-nicols observation (Fig. 1h). But, we observed a faint blue color in the first and third quadrants, suggesting that birefringence was weakened but it still showed positive birefringence (Fig. 1i). These results clearly show that the birefringence in the packed film can be controlled by changing the combination of particles with two different diameters. SEM images of the packing structures of the particles in the films in Fig. 1 are shown in Fig. 2. All SEM images were recorded at a position in which the film thickness was maximum in each sample. The particles packed in a random manner in the particulate film with $\alpha = 2.2$ (Fig. 2a). The larger particles were embedded in the packed smaller particles, as shown in Fig. 2b and c. We also confirmed that surface structure of binary particles varied depending on a position of a sample as shown in Fig. S2 in the ESI.† However, such small variation in packing structures did not affect color patterns of birefringence. The mixing effect on the birefringence was dependent on the volume ratios of the large and small particles. The birefringence of packed films of 100 nm and smaller particles are shown in Fig. 3. In samples of $\alpha = 2.2$, birefringent colors in packed films did not change so much (Fig. 3p–t). Conversely, in samples of $\alpha = 5.0$, birefringent colors were gradually weakened as φ_L increased from 0.1 to 0.7 (Fig. 3k–n). This suggests that positive birefringence was weakened by mixing of binary particles. Upon further increasing φ_L, positive birefringence appeared clearly again (Fig. 3o). When $\alpha = 8.3$, color of packed films was purple, and we did not observe any clear birefringent color. Thus birefringence was not detectable from $\varphi_L = 0.1$ to 0.5 (Fig. 3f–h). Negative birefringence was observed in the sample of $\varphi_L = 0.7$ (Fig. 3i). However, positive birefringence appeared again in the sample of $\varphi_L = 0.9$ (Fig. 3j). For samples of $\alpha = 20$, the films in Fig. 3b–d appeared dark, but this was caused by strong scattering of light. We used transmitted light to visualize the birefringence and we were not able to detect birefringence in these films because of scattering. Currently, we do not understand why mixed packing of large and small particles caused severe scattering of light, as in Fig. 3b–d, but this suggests a complicated interaction between visible light and packed films of binary particles. Conversely, apparent double ring birefringence was observed in the sample of $\varphi_L = 0.9$ as shown in Fig. 3e.

Birefringence of particulate films of 200 nm particles and smaller ones are shown in Fig. 4. We did not observe any clear

 This journal is © The Royal Society of Chemistry 2020

Open Access Article. Published on 14 January 2020. Downloaded on 9/23/2024 2:41:28 AM.
This article is licensed under a Creative Commons Attribution-NonCommercial 3.0 Unported Licence.

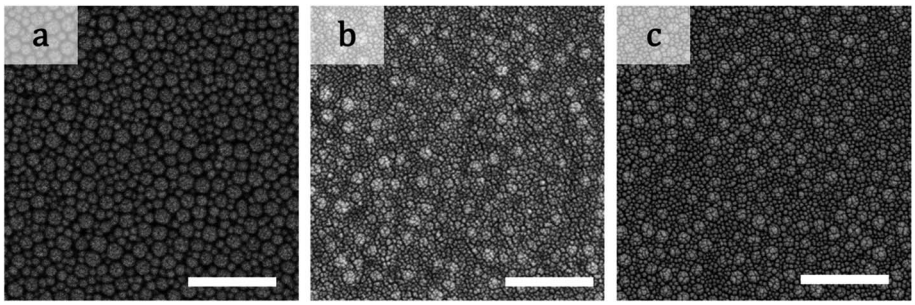

Fig. 2 SEM images of the films in (a) Fig. 1a, (b) Fig. 1d, and (c) Fig. 1g. The scale bars are 500 nm.

change in birefringence in the samples of $\alpha = 2.0$. Weakening of positive birefringence was observed in the samples of $\alpha = 4.4$ when φ_L increased from 0.1 to 0.7 as shown in Fig. 4p–s. Upon further increasing φ_L, clear color pattern of positive birefringence appeared again (Fig. 4t). Both weakening of positive birefringence and emergence of negative birefringence were observed in the samples of $\alpha = 10$ (Fig. 4k–o). For further increasing α, we prepared 10 samples as shown in Fig. 4a–j, but we were able to detect birefringence only in three samples (Fig. 4e, i and j). All three samples showed negative birefringence, including double-ring samples in Fig. 4e and j. SEM images of the films with φ_L of 0.7 and $\alpha = 2.0$, 4.4 and 10 are shown in Fig. 5. Similar to the images in Fig. 2, the large

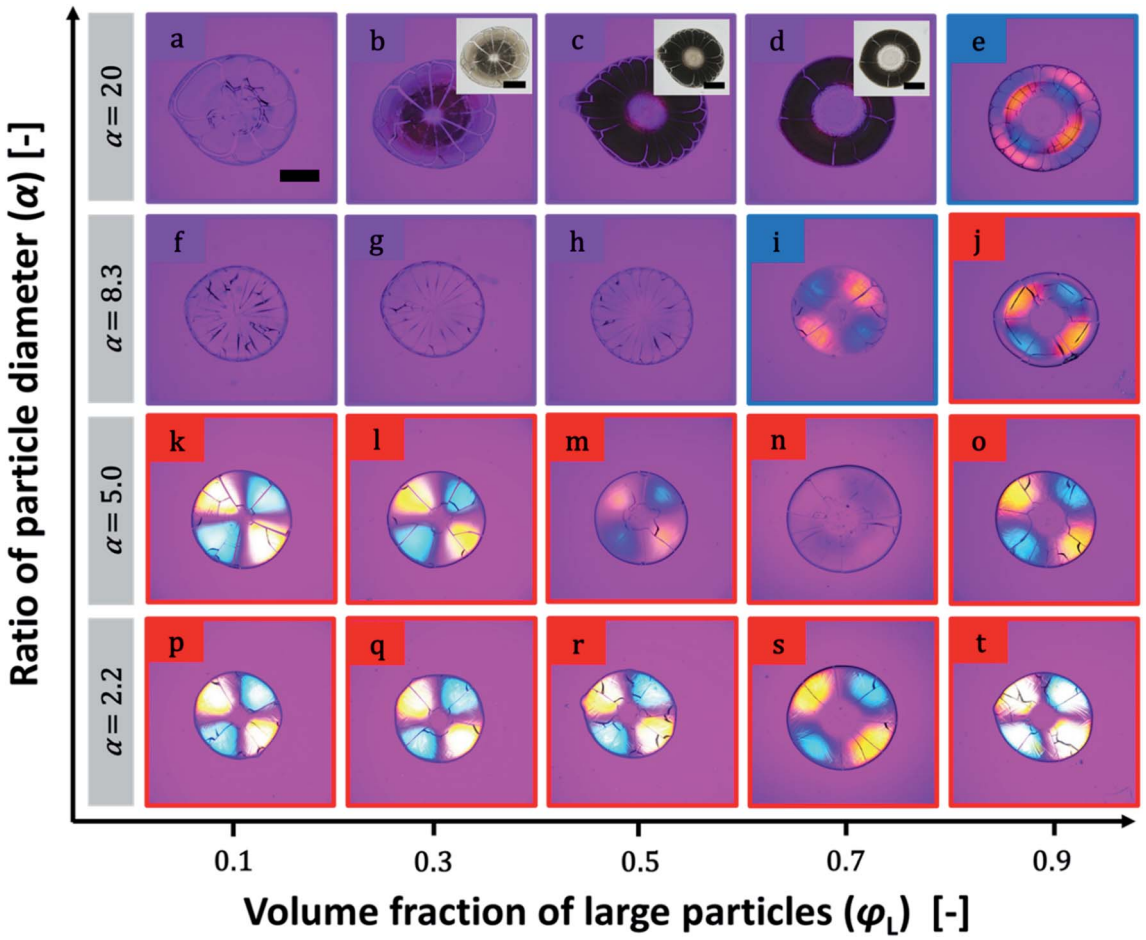

Fig. 3 Optical micrographs of packed films of 100 nm and smaller particles under birefringent observation. We changed φ_L and α. (a)–(e) $\alpha = 20$, (f)–(j) $\alpha = 8.3$, (k)–(o) $\alpha = 5.0$, and (p)–(t) $\alpha = 2.2$. Frame colors of images, which correspond to the background colors for alphabet (a)–(t) in images, stand for types of birefringence of samples: positive (red), negative (blue) and not detectable birefringence (purple), respectively. The insets in (b)–(d) show transmission optical microscope images of the same films. We note that the sample in (j) showed double-ring structure and we clearly observed positive birefringence in the inner ring. However, we did not observe any clear birefringent color except for purple in the outer ring. Therefore, it was categorized "positive". All of the scale bars are 500 μm.

Open Access Article. Published on 14 January 2020. Downloaded on 9/23/2024 2:41:28 AM.
This article is licensed under a Creative Commons Attribution-NonCommercial 3.0 Unported Licence.

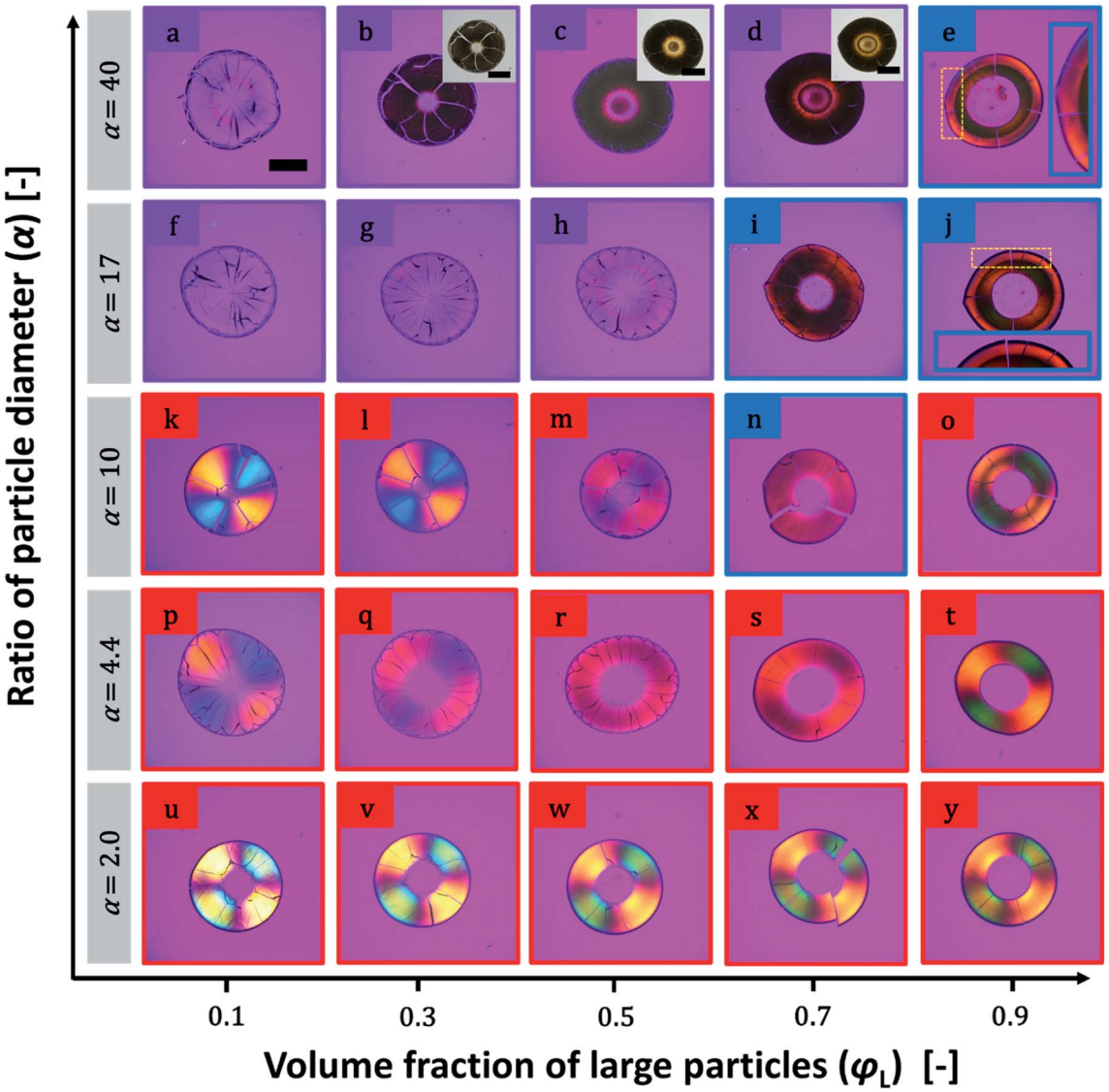

Fig. 4 Optical micrographs of packed films of 200 nm and smaller particles under birefringent observation. We changed the volume ratio of large particles φ_L and the diameter ratio α. (a)–(e) $\alpha = 40$, (f)–(j) $\alpha = 17$, (k)–(o) $\alpha = 10$, (p)–(t) $\alpha = 4.4$, and (u)–(y) $\alpha = 2.0$. Frame colors of images, which correspond to the background colors for alphabet (a)–(y) in images, stand for types of birefringence of samples: positive (red), negative (blue) and not detectable birefringence (purple), respectively. All of the scale bars are 500 μm. The insets in (b)–(d) show transmission optical microscope images of the same films. The insets in (e) and (j) showed enlarged images of parts of the samples, indicated by dotted boxes in the images. Both samples showed double ring birefringence. In the outer rings in (e) and (j), the first and third quadrants were brighter than in the second and forth quadrants, suggesting that the outer rings in these samples showed negative birefringence.

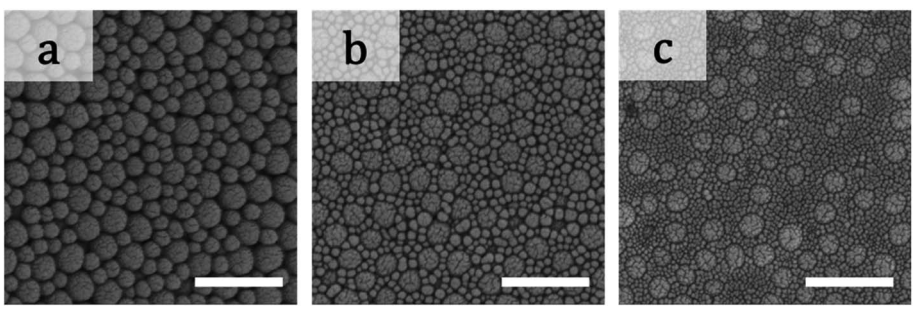

Fig. 5 SEM images of the films in (a) Fig. 4x, (b) Fig. 4s, and (c) Fig. 4n. The scale bars are 500 nm.

 This journal is © The Royal Society of Chemistry 2020

Open Access Article. Published on 14 January 2020. Downloaded on 9/23/2024 2:41:28 AM.
This article is licensed under a Creative Commons Attribution-NonCommercial 3.0 Unported Licence.

particles appeared to be embedded in the packed small particles.

The above films were all obtained by drying a suspension in which two types of particles were completely mixed before drying. We changed the drying procedure as follows. We first placed a suspension of large particles (100 nm) on a substrate. After drying for a desired period of time, we added a suspension of small particles (12 nm) to the drying suspension of large particles. When we added the suspension of small particles after drying the suspension for 30 s, negative birefringence appeared in the dried film (Fig. 6a). When we added the suspension of small particles after drying for 120 s, birefringence appeared, but in a complicated manner (Fig. 6b). We further investigated the mixture of particles in a different way. After the suspension of large particles completely dried, we placed a suspension of small particles on the film of large particles. The formed film showed positive birefringence (Fig. 6c). The same result was obtained when we added a suspension of large particles on a packed film of small particles (Fig. 6d). Thus, simultaneous packing of both large and small particles was necessary for changes in the birefringence.

3.2 Mechanism of positive and negative birefringence in packed films

In this work, we found that packed films of binary particles showed two types of birefringence: positive and negative birefringence (Fig. 1). Negative birefringence of a packed film of mixed binary particles was briefly reported in ref. 30, but the detailed mechanism was not investigated. In positive spherulites of packed particles with a mono-modal size distribution, the colloidal particles more tightly pack in the radial direction than in the circumferential direction.[30] Because of the smaller distance between the packed particles in the radial direction, the refractive index is larger than that in the other direction. Spontaneous flow of the drying suspension from the center to the edge of the cast droplet has been proposed to be the origin of the directional compression of packed particles.[30] The packed films of mixed particles showed negative birefringence (Fig. 1f). According to the same interpretation, negative birefringence means a larger refractive index in the circumferential direction than in the radial direction. This suggests that the particles were more tightly packed in the circumferential direction. We observed the suspension flow during drying and confirmed that there was no significant difference in the flow patterns in drying of binary colloidal suspensions. Therefore, suspension flow was not the origin of the change in the birefringence.

Another important issue is that there was an optimal volume ratio for the change in the birefringence. In these films, large particles were embedded in between packed small particles. The volume ratio of large particles affected the packing structure of particles, as shown in Fig. 7 in which we used binary colloids of 100 and 20 nm particles. The distance between the large particles was longer when the volume ratio of large particles was smaller, as shown in Fig. 7a–c. The large particles were embedded in packed small particles and isolated. In

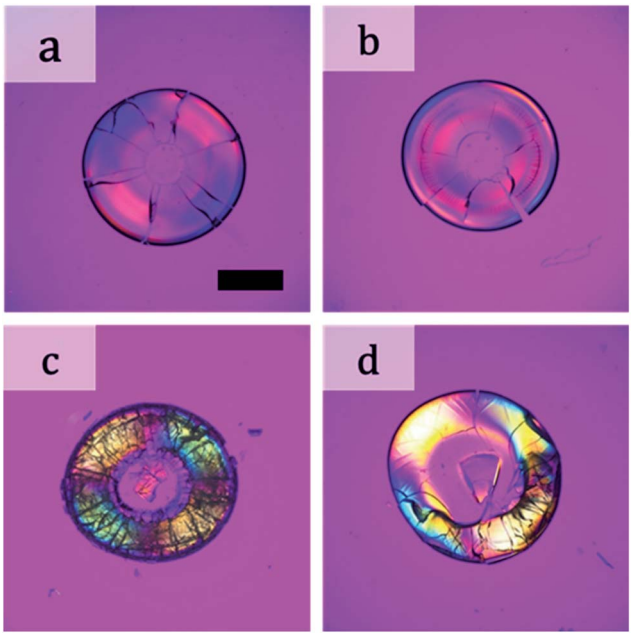

Fig. 6 Birefringence of packed films of 100 and 12 nm particles. Films formed by drying a suspension of 100 nm particles for (a) 30 s and (b) 120 s and then adding a suspension of 12 nm particles. (c) Film formed by adding a suspension of 12 nm particles to a completely dried suspension of 100 nm particles. (d) Film formed by adding a suspension of 100 nm particles to a complete dried suspension of 12 nm particles. The scale bar in (a) is 500 μm.

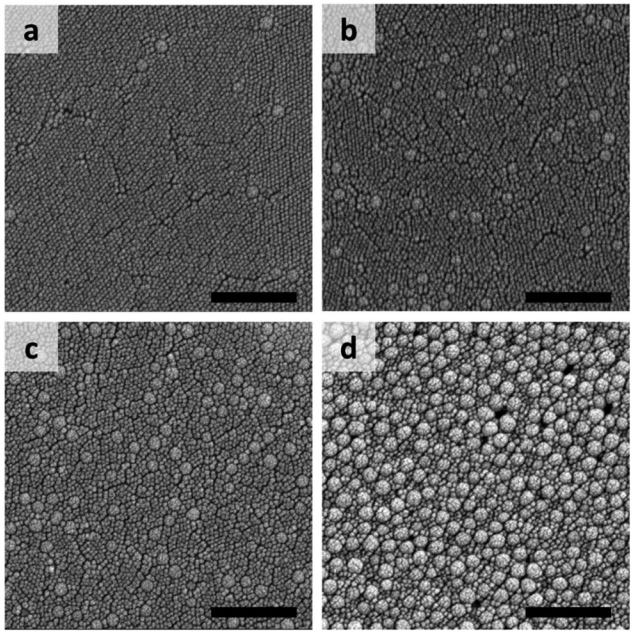

Fig. 7 SEM images of packed films of 100 and 20 nm particles with different volume ratios: (a) $\varphi_L = 0.1$, (b) $\varphi_L = 0.3$, (c) $\varphi_L = 0.5$, and (d) $\varphi_L = 0.9$. The film with $\varphi_L = 0.7$ is shown in Fig. 2c. All of the scale bars are 500 nm.

Open Access Article. Published on 14 January 2020. Downloaded on 9/23/2024 2:41:28 AM.
This article is licensed under a Creative Commons Attribution-NonCommercial 3.0 Unported Licence.

addition, a regular structure of small particles was observed. Thus, the large particles did not significantly disturb packing of small particles, and the birefringent property of the packed film was mainly determined by the small particles. In contrast, we did not observe any effect of addition of small particles when $\varphi_L = 0.9$ for $\alpha = 5.0$, although the small particles were packed between the large particles (Fig. 7d). In this case, the large particles mainly affected the birefringent property of the film, probably because of many direct contacts between large particles. On the basis of these results, we propose that packing of both large and small particles needs to be disturbed to show a change in the birefringence. In other words, a large particle does not directly contact other large particles, but the inter-particle distance between large particles should be small. In addition, the small particles should be packed between large particles. One possible packing structure is schematically illustrated in Fig. 8. This structure is strongly supported by the packing structure of the film that showed double ring birefringence (Fig. 3e). The inner positive birefringent part mainly consisted of packed large particles (Fig. 9b). In contrast, the small particles were packed between large particles and the distance between large particles was very small in the outer negative birefringent film (Fig. 9a). Therefore, such mixed packing of large and small particles is necessary for negative birefringence. The small particles were mainly observed in the outer ring. This is because small particles preferentially precipitate at the rim of the drying interface.[10,12,15] The volume ratio of small particles in Fig. 3e was 0.1 and almost all of the small particles were packed around the rim. Hence, the center of the packed film mainly consisted of large particles and positive birefringence was observed.

A large particle packs along the flow from the center to the edge. This induces directional packing of the particle. In the bulk material, directional compression causes expansion of the material, where the direction is normal to the compressive direction. The ratio of these distortions is defined as Poisson's ratio. Similar to this, the small particles pack between large particles, and radial compression would induce expansion of the packed layer of small particles to the circumferential direction, as shown in Fig. 10. This would result in a decrease in the packing distance between particles in the circumferential direction, which causes negative birefringence in packed films of binary particles, as shown in Fig. 1. However such conversion in compressive direction would not be easy to occur in particulate films and this would be a reason why we observed negative birefringence only in limited number of samples. The diameter ratio also affects the change in the birefringence. Because packing conditions gradually changed as the diameter ratio increases, negative birefringence or weakening of positive birefringence appeared as in Fig. 3 and 4. Further study on this point could provide a new insight in mechanical responses in packed-binary particulate films. Such study would be helpful to establish a theory to describe birefringence in packed spherical particles.

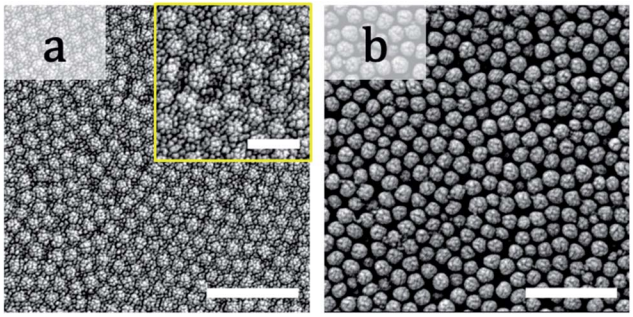

Fig. 9 SEM images of the (a) outer and (b) inner rings of the packed film in Fig. 3e. The scale bars are 500 nm. The inset in (a) is a magnified image of (a). The scale bar in the insert is 200 nm.

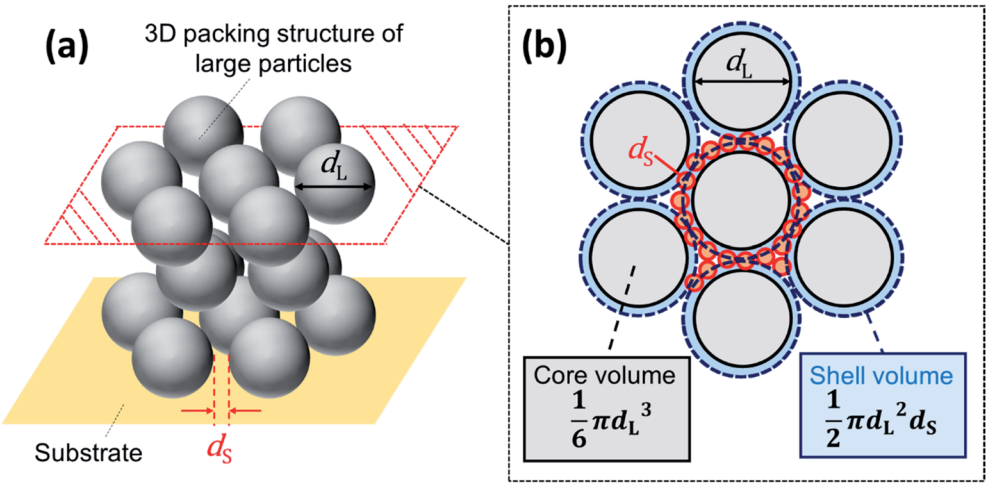

Fig. 8 Schematic illustrations of our model. (a) Three dimensional packing of large particles. We note that only large particles are sketched in (a) just for clarity. In our mode, a single layer of small particles forms between large particles, and the surface distance between each large particle is d_s. (b) A cross sectional image of packed binary particles on a plane indicated by the dotted red rectangular in the three-dimensional sketch in (a). A single shell layer of small particles forms around a large particle.

 This journal is © The Royal Society of Chemistry 2020

Open Access Article. Published on 14 January 2020. Downloaded on 9/23/2024 2:41:28 AM.
This article is licensed under a Creative Commons Attribution-NonCommercial 3.0 Unported Licence.

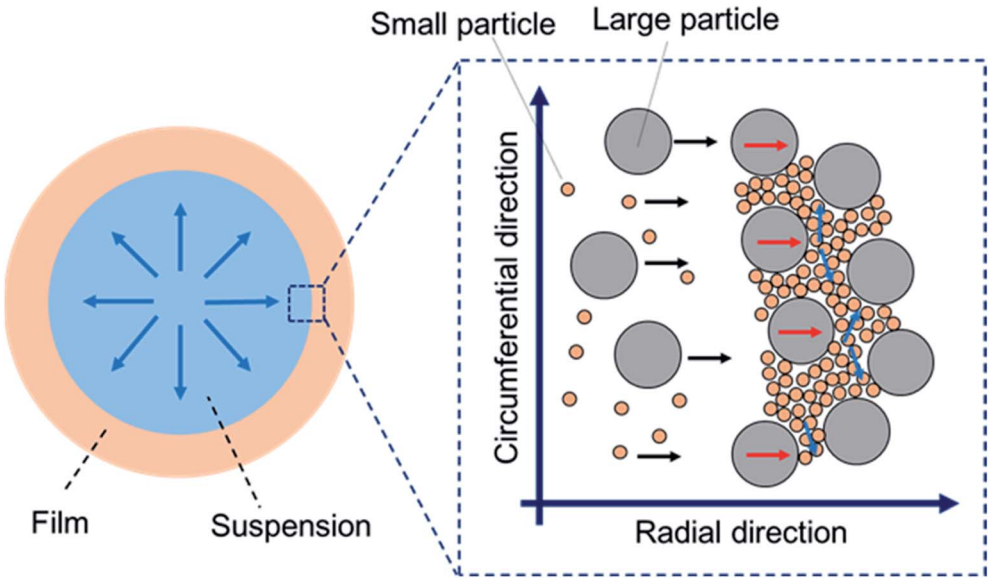

Fig. 10 Schematic illustration of formation of a film that shows negative birefringence.

3.3 Estimation of φ_L based on the proposed structure

We estimated the volume ratio required to form the structure shown in Fig. 8. Assuming that a single layer of small particles forms between the large particles, the volume of the shell of the small particles is approximately described by $\pi {d_L}^2 d_S/2$. The volume of a large particle is $\pi {d_L}^3/6$. Thus, the relation between the volumes and volume fractions is

$$\frac{1}{6}\pi {d_L}^3 \ : \ \left(\frac{1}{2}\pi {d_L}^2 d_S + \frac{1}{6}\pi {d_L}^3\right) = \varphi_L \ : \ (\varphi_L + \varphi_S), \qquad (1)$$

where φ_S is the dry-state volume fraction of the small particles in packed films. From eqn (1), $\varphi_S = 3(d_S/d_L)\varphi_L$. The sum of φ_L and φ_S is 1. In addition, from our definition of the diameter ratio, $d_S/d_L = \alpha^{-1}$. Thus, we finally obtain the following relation:

$$\varphi_L = \alpha/(3 + \alpha) \qquad (2)$$

From this relation, we obtained $\varphi_L \approx 0.77$ for $\alpha = 10$ and $\varphi_L \approx 0.63$ for $\alpha = 5$. These are only approximations, but they suggest that the volume fraction should be about 0.7 to form the packed structure in Fig. 8. We consider that this is one of the reasons why negative and weakened positive birefringence most clearly appeared at about $\varphi_L = 0.7$. In addition, we analyzed SEM image of the sample in Fig. 9a to estimate the actual volume fraction of large particles in the outer ring. SEM image provides an area fraction of large particles but we need to convert it to a volume fraction of large particles in packed binary particles. Assuming the radius of large particles as $d_L/2$ and large particles packed in a square area of H^2, then an area fraction of packed large particles on the surface of packed layer, f_S, is estimated as $f_S = \pi(d_L/2)^2 N_S/H^2$, in which N_S is the number of large particles packed in the square. In a cubic box with a volume of H^3, the number of packed particles in the box N_V is roughly $N_V \sim (H/d_L)N_S$. Therefore the total volume of large particles in the box, V_{LP}, is $V_{LP} \sim (\pi {d_L}^3/6)N_V$. We consider packing of binary spherical particles. The total volume fraction that is occupied by spherical particles in the box is roughly 0.7. Therefore the volume fraction of large particles φ_L is estimated as $V_{LP}/(0.7H^3) \sim 20 f_S/21$. The area fraction of large particles f_S in the outer ring obtained from Fig. 9a was 0.82 and this suggests $\varphi_L \sim 0.8$. Conversely, our model predicts $\varphi_L = 0.87$ for binary particles of $\alpha = 20$. This reasonable agreement also supports our model. These results suggested that a packing structure in which large particles are packed but separated by a packed thin layer of small particles would be necessary.

Drying of colloidal suspensions with a binary size distribution has been extensively studied. One of the main points in these studies is spontaneous segregation of the smaller particles around the drying interface. However, our results revealed that staggered packing of large and small particles is also a candidate to show a new property in the packed film. Thus, we consider that investigating the drying process in which mixed packing of large and small particles spontaneously occurs is important to produce functional packed films of binary particles.

4. Conclusions

We have demonstrated that positive and negative birefringence emerged in films of packed binary colloidal particles. Positive birefringence was observed when α was small. In contrast, negative birefringence or weakening of positive birefringence was clearly observed in films with a large α and an optimal volume fraction of large particles. We propose a staggered packing structure of large and small particles as the origin of the observed change in birefringence. The volume ratio of large particles required to form a single shell layer of small particles around a large particle was estimated to be about 0.7. This estimated value was in reasonable agreement with the experimental data. Our results suggest that precise control of the

Open Access Article. Published on 14 January 2020. Downloaded on 9/23/2024 2:41:28 AM.
This article is licensed under a Creative Commons Attribution-NonCommercial 3.0 Unported Licence.

packing structures of binary particles has the potential to form functional materials.

Conflicts of interest

There are no conflict to declare.

Acknowledgements

This work was partially supported by JSPS KAKENHI (grant number: 16H02413). We thank Prof. H. Kamiya for his permission to access the FE-SEM and DLS equipment. We thank Tim Cooper, PhD, from Edanz Group (www.edanzediting.com/ac) for editing a draft of this manuscript.

References

1 L. Goehring, J. Li and P.-C. Kiatkirakajorn, *Philos. Trans. R. Soc., A*, 2016, **375**, 20160161.
2 S. Portal-Marco, M.-À. Vallvé, O. Arteaga, J. Ignés-Mullol, C. Corbella and E. Bertran, *Colloids Surf., A*, 2012, **401**, 38–47.
3 J. H. Moon and S. Yang, *Chem. Rev.*, 2010, **110**(1), 547–574.
4 E. Avci and M. Culha, *RSC Adv.*, 2013, **3**, 17829–17836.
5 S. Lim, K. H. Ahn and M. Yamamura, *Langmuir*, 2013, **29**(26), 8233–8244.
6 S. Lim, S. Kim, K. H. Ahn and S. J. Lee, *Ind. Eng. Chem. Res.*, 2015, **54**(23), 6146–6155.
7 L. H. Mujawar, J. G. M. Kuerten, D. P. Siregar, A. van Amerongen and W. Norde, *RSC Adv.*, 2014, **4**, 19380–19388.
8 C. Zhang and P. Akcora, *RSC Adv.*, 2017, **7**, 18321–18326.
9 M. Schulz and J. L. Keddie, *Soft Matter*, 2018, **14**, 6181–6197.
10 E. Hendarto and Y. B. Gianchandani, *J. Micromech. Microeng.*, 2013, **23**, 075016.
11 D. K. Makepeace, A. Fortini, A. Markov, P. Locatelli, C. Lindsay, S. Moorhouse, R. Lind, R. P. Sear and J. L. Keddie, *Soft Matter*, 2017, **13**, 6969–6980.
12 W. Liu, J. Midya, M. Kappl, H.-J. Butt and A. Nikoubashman, *ACS Nano*, 2019, **13**(5), 4972–4979.
13 O. Cusola, S. Kivistö, S. Vierros, P. Batys, M. Ago, B. L. Tardy, L. G. Greca, M. B. Roncero, M. Sammalkorpi and O. J. Rojas, *Langmuir*, 2018, **34**(20), 5759–5771.
14 V. H. Chhasatia and Y. Sun, *Soft Matter*, 2011, **7**, 10135–10143.
15 N. D. Patil, R. Bhardwaj and A. Sharma, *Langmuir*, 2018, **34**(40), 12058–12070.
16 B. M. Weon and J. H. Je, *Phys. Rev. E: Stat., Nonlinear, Soft Matter Phys.*, 2013, **87**, 013003.
17 M. Parsa, S. Harmand and K. Sefiane, *Adv. Colloid Interface Sci.*, 2018, **254**, 22–47.
18 F. Buss, C. C. Roberts, K. S. Crawford, K. Peters and L. F. Francis, *J. Colloid Interface Sci.*, 2011, **359**, 112–120.
19 N. R. Devlin, K. Loehr and M. T. Harris, *AIChE J.*, 2015, **61**(10), 3547–3556.
20 K. Katagiri, Y. Tanaka, K. Uemura, K. Inumaru, T. Seki and Y. Takeoka, *NPG Asia Mater.*, 2017, **9**, e355.
21 H. Fudouzi and Y. Xia, *Langmuir*, 2003, **19**(23), 9653–9660.
22 J. D. Forster, H. Noh, S. F. Liew, V. Saranathan, C. F. Schreck, L. Yang, J.-G. Park, R. O. Prum, S. G. J. Mochrie, C. S. O'Hern, H. Cao and E. R. Dufresne, *Adv. Mater.*, 2010, **22**, 2939–3944.
23 A. Kawamura, M. Kohri, S. Yoshioka, T. Taniguchi and K. Kishikawa, *Langmuir*, 2017, **33**(15), 3824–3830.
24 T. Iwasaki, Y. Tamai, M. Yamamoto, T. Taniguchi, K. Kishikawa and M. Kohri, *Langmuir*, 2018, **34**(39), 11814–11821.
25 Z. Dai, Y. Li, G. Duan, L. Jia and W. Cai, *ACS Nano*, 2012, **6**(8), 6706–6716.
26 M. Mittal and E. M. Furst, *Adv. Funct. Mater.*, 2009, **19**, 3271–3278.
27 R. Duggal, F. Hussain and M. Pasquali, *Adv. Mater.*, 2006, **18**, 29–34.
28 T. Scharf, *Polarized light in liquid crystals and polymers*, Wiley, 2007.
29 S. Inasawa and Y. Yamaguchi, *Langmuir*, 2009, **25**(18), 11197–11201.
30 K. Yamaguchi, S. Inasawa and Y. Yamaguchi, *Phys. Chem. Chem. Phys.*, 2013, **15**, 2897–2902.
31 H. Miyazaki, K. Abe and S. Inasawa, *Drying Technol.*, 2020, **38**(3), 385–394.

 This journal is © The Royal Society of Chemistry 2020